Review

CellPress

Bioprinting for cancer research

Stephanie Knowlton[1*], Sevgi Onal[1*], Chu Hsiang Yu[2], Jean J. Zhao[3,4], and Savas Tasoglu[1,2]

[1] Department of Biomedical Engineering, University of Connecticut, 260 Glenbrook Road, Storrs, CT 06269, USA
[2] Department of Mechanical Engineering, University of Connecticut, 191 Auditorium Road, Storrs, CT 06269, USA
[3] Department of Biological Chemistry and Molecular Pharmacology, Harvard Medical School, 25 Shattuck Street, Boston, MA 02115, USA
[4] Cancer Biology, Dana–Farber Cancer Institute, 450 Brookline Avenue, Boston, MA 02215, USA

Bioprinting offers the ability to create highly complex 3D architectures with living cells. This cutting-edge technique has significantly gained popularity and applicability in several fields. Bioprinting methods have been developed to effectively and rapidly pattern living cells, biological macromolecules, and biomaterials. These technologies hold great potential for applications in cancer research. Bioprinted cancer models represent a significant improvement over previous 2D models by mimicking 3D complexity and facilitating physiologically relevant cell–cell and cell–matrix interactions. Here we review bioprinting methods based on inkjet, microextrusion, and laser technologies and compare 3D cancer models with 2D cancer models. We discuss bioprinted models that mimic the tumor microenvironment, providing a platform for deeper understanding of cancer pathology, anticancer drug screening, and cancer treatment development.

Application of bioprinting to cancer research

Cancer remains one of the most predominant life-threatening diseases in the world, with 14 million new cases of cancer and 8.2 million cancer-related deaths worldwide in 2012. The annual number of cases is predicted to rise from 14 million to 22 million over the next two decades [1]. The economic burden in the USA was US$88.7 billion in 2011 based on direct medical costs alone [American Cancer Society (2015) Economic impact of cancer (http://www.cancer.org/cancer/cancerbasics/economic-impact-of-cancer)]. There are hundreds of known types of cancer and the disease is highly complex even within a single cancer type, making the development of a single cure an astronomical task [2,3]. To gain a better understanding of cancer genesis and progression, there is a need for more complex and physiologically relevant 3D cancer models that closely mimic the *in vivo* tumor microenvironment. In light of these challenges, bioprinting offers the ability to form highly controllable cancer tissue models and shows potential to significantly accelerate cancer research.

2D cancer models are widely used for cancer research, contributing to our basic knowledge of cancer biology. Protein expression [4], gene expression [5], protein gradient profiles and cell signaling [6,7], migration [8], morphology [9], proliferation [10], viability [9], organization [9], and drug response [11,12] have been shown to differ between 2D and 3D cancer models [6,13]. Although 2D cultures offer hypothetical results regarding cancer pathogenesis, it is necessary to expose cancer cells to the cell–cell and cell–matrix interactions they would experience *in vivo* to achieve more physiologically relevant results. Thus, cancer studies using 3D models have achieved more accurate representations of cancer tissues in terms of tumor microenvironment and biological behavior with controlled spatial distribution of cells, which is crucial for developing early diagnosis and treatment strategies for cancer.

3D printing is an additive manufacturing process by which precursor materials are deposited layer by layer to form complex 3D geometries from computer-aided designs [14–16]. A notable advantage of 3D printing is that complex architectures may be printed with efficiency and customizability either on an industrial scale or on a desktop-printing scale. 3D printing has more recently been developed into a process called bioprinting in which living cells, extracellular matrix (ECM) components, biomaterials, and biochemical factors are printed onto a receiving substrate or liquid reservoir [17–20]. The interest in bioprinting has significantly grown within the scientific and medical communities due to several key advantages over previously accepted fabrication methods such as photolithography, soft lithography, and microstamping. These advantages include the ability to create geometrically complex scaffolds containing viable cells [18,19,21], efficiency, low cost [22], high throughput [23], precise reproducibility [18], and limited need for specialized training. High-throughput fabrication of 3D structures is currently limited with traditional microfabrication techniques that generate 2D building blocks and rely on layer-by-layer assembly to form 3D structures [24–32]. Current methods for co-culturing multiple cell types in desired configurations lack high-throughput capabilities, demanding multiple labor-intensive fabrication steps [23], but spatial patterning of different cell types or ECM components is possible using various 'bio-inks' for printing [33]. With these unique advantages, bioprinting offers a broad range of applications including biochemical surface patterning and *in situ* printing of biomaterials for wound healing as well as designing 3D tissue constructs for basic research,

Corresponding author: Tasoglu, S. (savas@engr.uconn.edu).
*These authors contributed equally to this work.

0167-7799/
 http://dx.doi.org/10.1016/j.tibtech.2015.06.007

Table 1. Comparison of common bioprinting technologies

Performance metric	Microextrusion bioprinting	Laser-assisted bioprinting	Inkjet bioprinting	Refs
Throughput	Medium	Low to medium	High	[23]
Droplet size	5 μm to millimeters wide	>20–80 μm	50–300 μm	[23,55,88]
Spatial resolution	Medium	Medium to high	Medium	[23]
Single-cell encapsulation control	Medium	Medium to high	Low	[23]
Cell viability	40–80%	>95%	>85%	[55]
Cell density	High	Medium, 10^8 cells/ml	Low, $<10^6$ cells/ml	[55]
Material/hydrogel viscosity	30 mPa.s to > 600 kPa.s	1–300 mPa.s	<10 mPa.s	[37,55]
Gelation method	Chemical, ionic, enzymatic, photocrosslinking, shear thinning, thermal, pH	Ionic	Ionic, enzymatic, photocrosslinking, thermal	[89]
Gelation speed	Medium	High	High	[89]
Print/fabrication speed	High	Low	Medium	[89]
Printer cost	Medium	High	Low	[55]

regenerative medicine, disease modeling, or pharmaceutical research.

This review focuses on recent advances in the use of bioprinting technologies for cancer research, bioprinting physiologically relevant testing platforms for anticancer drug development, and computational modeling for improving bioprinting techniques.

Bioprinting techniques applied to 3D tumor models

Within the field of bioprinting, there are several strategies by which biological organization and complexity have been successfully modeled: inkjet-based [34,35], microextrusion [36–39], and laser-assisted bioprinting [40–44] (Table 1). Inkjet-based bioprinting involves generating droplets of bio-ink at the print head assisted by either a heater or a piezoelectric actuator (Figure 1A). Microextrusion bioprinting can be achieved using either pneumatic [36–39] or mechanical (piston or screw driven) forces [36–39,45–47] to extrude a continuous stream of a bio-ink (Figure 1B). Laser-assisted bioprinting can be conducted by two methods: laser guided or laser induced. In the laser-guided direct cell-printing method, a laser beam is directed into a cell suspension. The difference in refractive indices of cells and cell media enables a laser beam to trap and guide cells onto a receiving substrate [40,48] (Figure 1C). In the laser-induced bioprinting method, which is more common, a cell-laden hydrogel is deposited below a laser-absorbing layer that is used as a donor film and placed parallel to a receiving substrate (Figure 1D). Cell-encapsulating hydrogel droplets are transferred from the donor film to the receiving substrate due to the heat transfer from a laser pulse to the donor film and the pressure of a laser-induced vapor bubble [42,44,49,50]. Stereolithography, which involves curing a photoreactive material using light, has also been used for bioprinting. Digital micromirror projection printing uses a digital micro-mirror device to reflect UV light in a particular spatial pattern into a photopolymerizable macromer solution (Figure 2A) [51]. In this way, cells can be encapsulated in and seeded on 3D-patterned hydrogel scaffolds with a range of printable materials and control over microarchitecture and scaffold properties.

Two-step biofabrication

One method of bioprinting is a 'two-step' biofabrication method in which cell seeding is performed after 3D printing of the scaffold. Bioprinting can be used to generate precise biocompatible scaffolds for culturing cells with controllable structural features and composition. Digital micromirror device-based projection printing has been used to fabricate 3D polyethylene glycol (PEG) scaffolds with log-pile microarchitecture (Figure 2B–F) [52]. The elastic modulus of the scaffold was controlled by varying the PEG concentration without altering the structural or mechanical properties, allowing the effects of stiffness to be isolated and examined. Normal breast epithelial cells and Twist-transformed oncogenic cells were seeded onto the scaffold to study cell migration patterns. Cells cultured in 2D showed no statistical difference in migration on substrates with different stiffness. However, cells on 3D scaffolds demonstrated varying displacement, velocity, and path straightness depending on the scaffold stiffness and the presence of the Twist oncogene (Figure 2G–L). These results suggest that further research regarding cancer cell migration must be conducted in 3D systems.

One-step biofabrication

While 3D models can be generated via top-down methods by seeding cells into prefabricated scaffolds, there are limitations on controlling cell density, repeatability, spatial control, and scalability with this method [23]. In contrast to two-step bioprinting, one-step bioprinting methods print a mixture of hydrogel and cells, providing a more efficient way of fabricating 3D tissue models with less user input required [53]. A recent bioprinting technique has been shown to enable 3D patterning of human ovarian cancer (OVCAR-5) cells and normal fibroblasts on Matrigel™ with 3D complexity and spatial control over the microenvironment in terms of cell density and cell–cell distance [54]. This approach uses an automated XYZ stage with a dual ejector to position cell-encapsulating droplets at predefined locations on a substrate for high-throughput printing with high viability. OVCAR-5 cells were shown to proliferate and ultimately form acini (lobular structures) (Figure 3). Design parameters such as droplet ejection

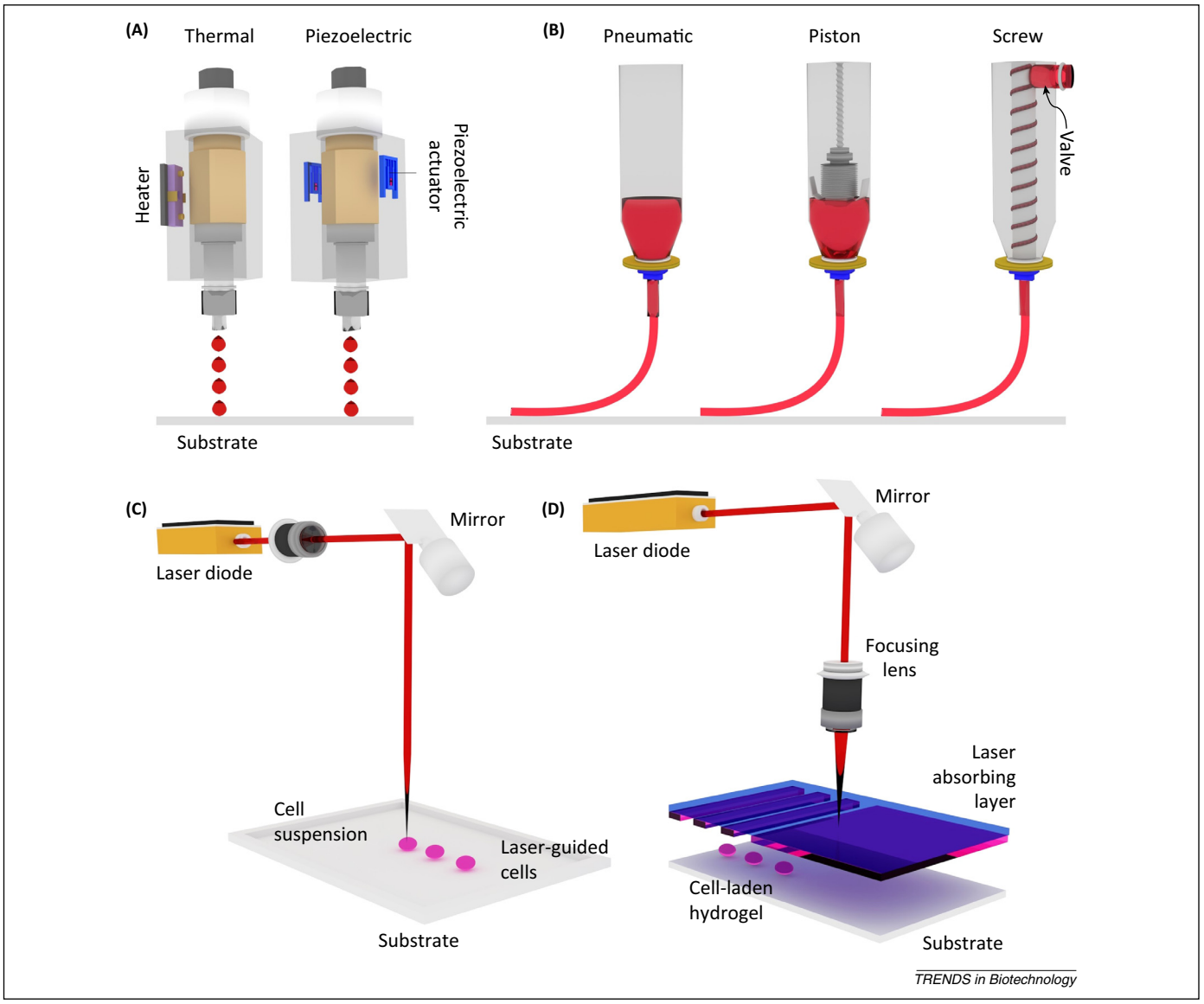

Figure 1. Inkjet, microextrusion, and laser-assisted bioprinting technologies. **(A)** Thermal and piezoelectric inkjet printing: Thermal inkjet printers are configured with a heater creating air-pressure pulses to generate droplets at the printhead. In piezoelectric inkjet printing, an actuator produces a mechanical pulse to force the bio-ink from the nozzle as droplets. **(B)** Microextrusion printers in the form of pneumatic, piston-driven, or screw-driven robotic dispensing systems. Instead of droplets, a continuous stream of hydrogel containing cells is dispensed. **(C)** Laser-guided direct cell printing: The difference in the refractive indices of cells and cell media forces photons from the laser beam to trap and guide cells onto a receiving substrate. **(D)** Laser-induced direct cell printing: The laser is focused on an absorbing layer and induces a vapor bubble through cell-laden hydrogel to transfer cell-encapsulating hydrogel droplets onto a substrate.

velocity, cell concentration, and culture duration were observed to affect acini growth kinetics after patterning. This technique accelerates the fabrication of cancer co-culture models for systematic investigation of cell–cell interactions. Once regulatory mechanisms between tumor cells and their microenvironment are better understood, high-throughput and reliable drug screening can be accomplished using models fabricated using the approach presented by this study.

Constructing *in vitro* tissue models using 3D bioprinting of cells and ECM is advantageous for mimicking the biological environments of living systems. Bioprinted 3D models enhance studies regarding disease pathogenesis and drug testing. An example is a recent 3D printing method for the construction of *in vitro* cervical tumor models in which HeLa cells were encapsulated within a hydrogel mixture of gelatin, alginate, and fibrinogen [12]. In this study, HeLa cells were 3D printed with ECM materials for comparison with controls cultured in conventional 2D models. Comparison of results obtained from 2D and 3D tumor models showed differences in cell proliferation, matrix metalloproteinase (MMP) protein expression, and the chemoresistance of the cells. Over 90% cell viability was achieved in the 3D bioprinted model and the cells proliferated at a higher rate than in 2D culture. HeLa cells in 3D also formed 3D cellular spheroids in contrast to the monolayer cell sheets formed in 2D culture. These differences may originate from cell–cell and cell–matrix interactions present in 3D culture conditions. MMP protein expression in HeLa cells was also shown to be higher in 3D printed models, most likely due to the functionality of MMPs in ECM degradation

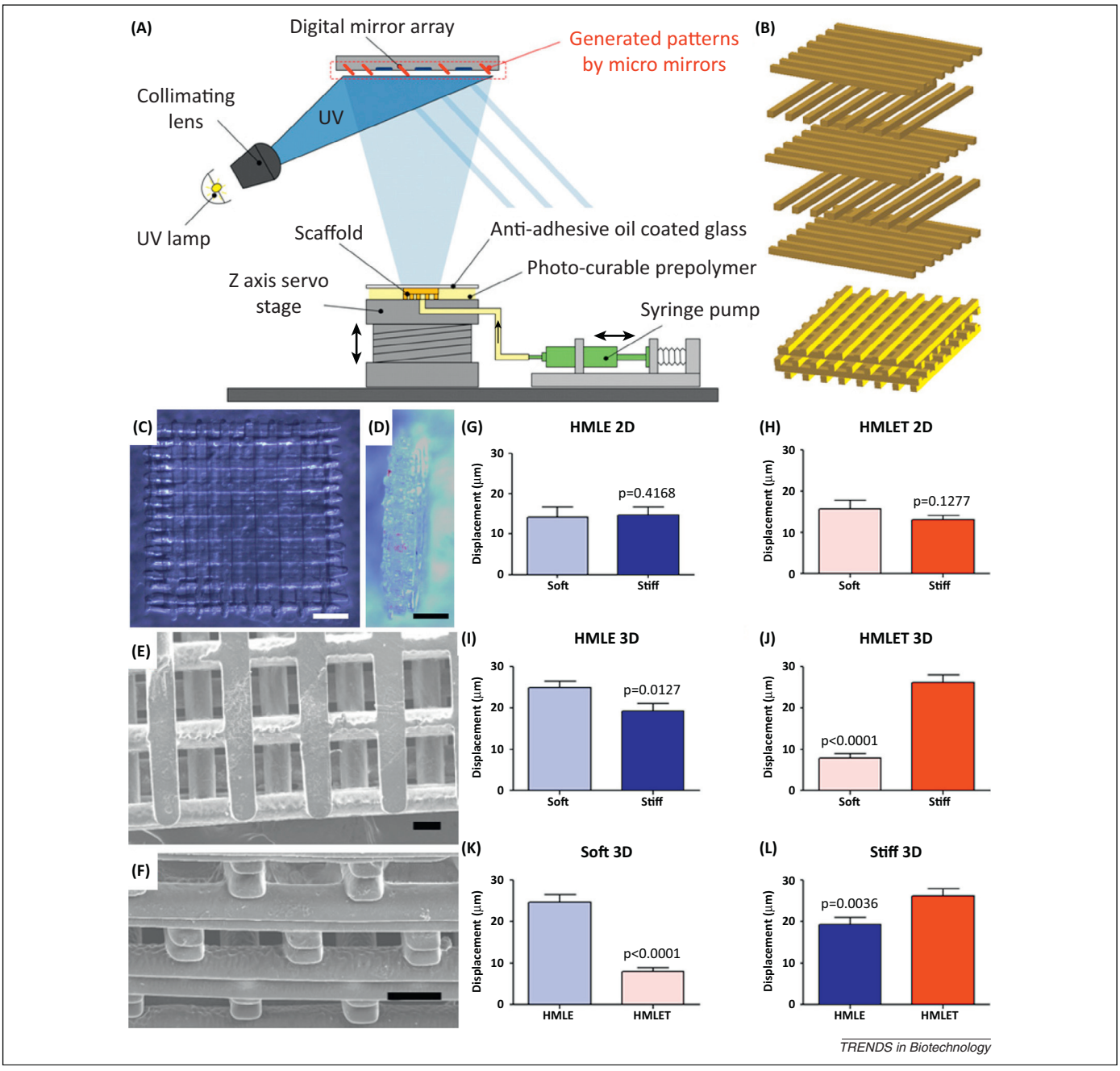

Figure 2. Digital micromirror-based projection printing (DMD-PP) for fabricating polyethylene glycol (PEG) log-pile structures. **(A)** Mechanism of DMD-PP, involving exposure of a photocurable PEG prepolymer to UV light in patterns generated by a digital micromirror array. **(B)** Crosslinked PEG structures are formed layer by layer by moving the stage along the z-axis between layers. Sequential formation of PEG layers forms a 3D log-pile scaffold. **(C)** Top and **(D)** side views of a five-layer PEG log-pile structure. Scale bar, 500 μm. **(E)** Top and **(F)** side view SEM images of the 3D log-pile scaffold. Scale bar, 100 μm. Measured displacement of **(G)** normal mammary epithelial cells (HMLE) and **(H)** TWIST modified cells (HMLET) in 2D culture. Measured displacement of **(I)** HMLE and **(J)** HMLET cells on 3D scaffolds. Measured displacement of HMLE and HMLET cells on **(K)** soft and **(L)** stiff 3D scaffolds. Reproduced, with permission, from [52].

(Figure 4). Cells in 3D printed constructs also exhibited a higher chemoresistance against paclitaxel treatment compared with that in 2D culture. The results of this study using a novel 3D cell-printing technique to construct *in vitro* tumor models help to better characterize tumor formation, progression, and response to anticancer treatments [12].

Scaffold-free approaches

Another approach is scaffold-free bioprinting, involving the fusion and self-assembly of multicellular spheroids [53,55]. ECM components significantly affect tumor cell behavior, including the mode of cell migration and cell dissemination, via cell–matrix interactions [56,57]. When heterogeneous 3D tumor models with multiple cell types are constructed via scaffold-free bioprinting, cells that are co-printed with tumor cells are used to naturally produce ECM, avoiding the problem of structural differences between the proteins used and the varying composition and material properties associated with exogenous scaffolds [58]. Thus, independent physiological interactions between cells and matrix can be more directly understood.

In a recent study using a scaffold-free method, breast cancer neotissues (newly formed tissues) were bioprinted

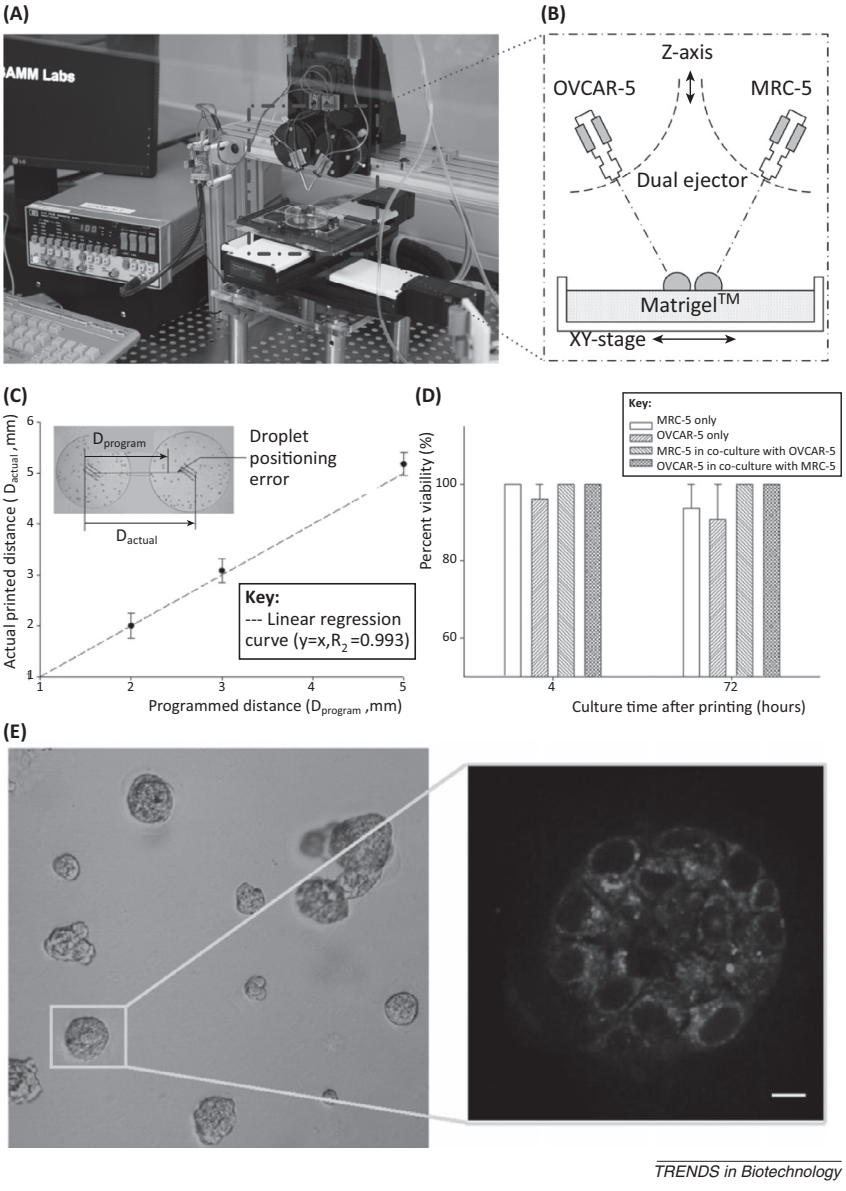

Figure 3. The construction and characterization of a high-throughput cell-patterning platform for printing a 3D *in vitro* ovarian cancer co-culture model. **(A)** A high-throughput ejector platform comprising a computerized stage and two ejectors is installed in a sterile hood to prevent contamination using HEPA filters. **(B)** Dual ejector heads are used to eject different cell types – ovarian cancer cells (OVCAR-5) and fibroblasts (MRC-5) – simultaneously onto a Matrigel™ substrate. **(C)** Droplet positioning accuracy of the high-throughput cell-patterning platform. The positioning error of two droplets is measured by the difference between the programmed distance ($D_{program}$) and the actual printed distance of droplets after patterning (D_{actual}); $R^2 = 0.9932$. **(D)** Percentage viability of OVCAR-5 and MRC-5 co-culture after printing (4 h) and at day 3 (72 h) with respect to flask cell viability ($n = 4$). **(E)** 3D acini formation in Matrigel. Two-photon autofluorescence images show the 3D structure of acini formed from OVCAR-5 cells 7 days following printing. Scale bar, 20 μm. Reproduced, with permission, from [54].

without a supportive scaffold [58]. Breast cancer cells were deposited along with fibroblasts, adipocytes, and endothelial cells in spatially definitive patterns to mimic breast tumor stroma. In these models, stromal cells were shown to secrete ECM, growth factors, and hormones, resulting in natural localization and function of the cells in a biomimetic tumor microenvironment. The bioprinted neotissues remained viable for more than 14 days and differentiation of adipocytes and formation of endothelial networks were observed. Histomorphological analysis showed adipose, stromal, epithelial, and carcinoma compartmentalization. 3D neotissue models were more resistant to chemotherapeutic agents compared with 2D-cultured cancer cells. Thus, these 3D neotissue models were validated as another useful tool for representing *in vivo* microenvironmental conditions and screening new anticancer therapies [58].

Optimizing cell viability

Cell survival rate after printing may be optimized by adjusting printing parameters such as applied pressure, nozzle diameter and temperature (in techniques using a nozzle), viscosity of the suspending medium, and environmental conditions [12,59]. Other parameters such as deformation of cell-encapsulating droplets, surface tension, and the hydrophobicity/hydrophilicity of the substrate have also been identified and evaluated via computational simulation and modeling. Further advanced computational

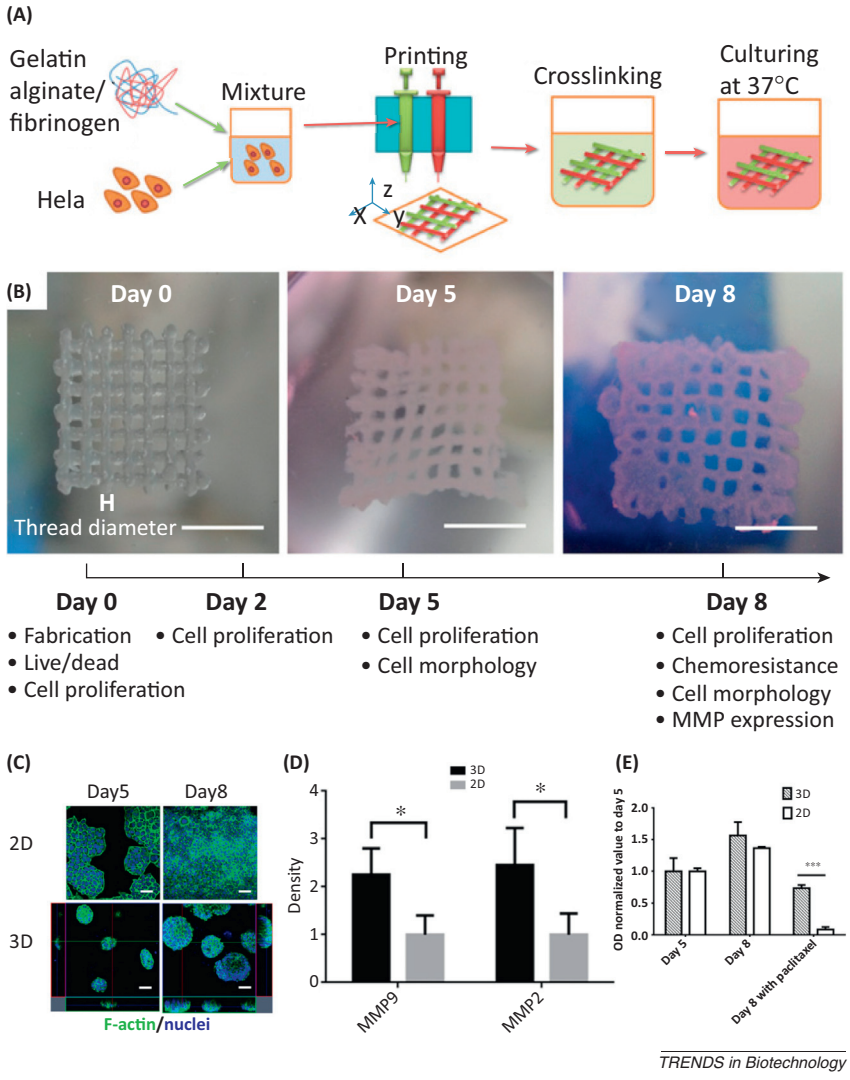

Figure 4. 3D printing method for HeLa cells and characterization compared with 2D planar culture. **(A)** Workflow of the 3D cell-printing process to fabricate 3D HeLa/hydrogel constructs. **(B)** Top view of 3D HeLa/hydrogel constructs on day 0, day 5, and day 8. Scale bar, 5 mm. **(C)** Cellular morphological changes were characterized by staining cell filaments and nuclei on day 5 and day 8 in 3D constructs and 2D planar cultures. Scale bar, 50 μm. **(D)** Semiquantitative analysis of matrix metalloprotease (MMP)-2 and -9 secretion shows the difference in MMP secretion of HeLa cells in 3D constructs versus 2D planar culture. $*P < 0.05$; *t*-test. **(E)** Chemoresistance of HeLa cells in 3D HeLa/hydrogel constructs and 2D planar culture on day 5 (the time of first addition of paclitaxel) and after paclitaxel treatment, as measured by cellular metabolic activity. Reproduced, with permission, from [12].

models can help researchers by identifying experimental conditions (such as the material properties of the encapsulating and surrounding media and ejection velocity), directing future research toward optimal viability. One additional important parameter is the duration of the bioprinting process. The viability of encapsulated cells is impacted by: (i) the waiting time of cells within the pre-gel bio-ink during fabrication; (ii) the waiting time of cells within the deposited construct during fabrication before incubation; and (iii) the sensitivity of different cell types to these external stresses. One potential approach to maximize viability is to use multinozzle printheads [60], which co-print cell-laden hydrogels simultaneously, decreasing the printing time [59].

Computational modeling for bioprinting

Computational simulations coupled with experimental tests can help in understanding the effects of experimental printing parameters on post-printing cell viability. Modeling and experimenting with double emulsion systems, which are fluid systems of emulsion droplets enclosing smaller inner droplets [61,62], are promising to develop a better understanding of the cell-printing process. A recent study combining experimental investigation with computational simulation revealed an intensification of the transient deformation oscillation of a double emulsion droplet under shear caused by the hydrodynamic effects of the inner droplet [61]. The inner droplet co-induces enhancing and suppressing effects on the deformation of the double emulsion droplet. These competing effects cause the double emulsion droplet to experience both larger and smaller steady deformation compared with the single-phase droplet. The dominant regime of the competing effects on deformation is determined by the ratio of the inner droplet radius to the outer droplet radius and the capillary number, representing the competition of viscous

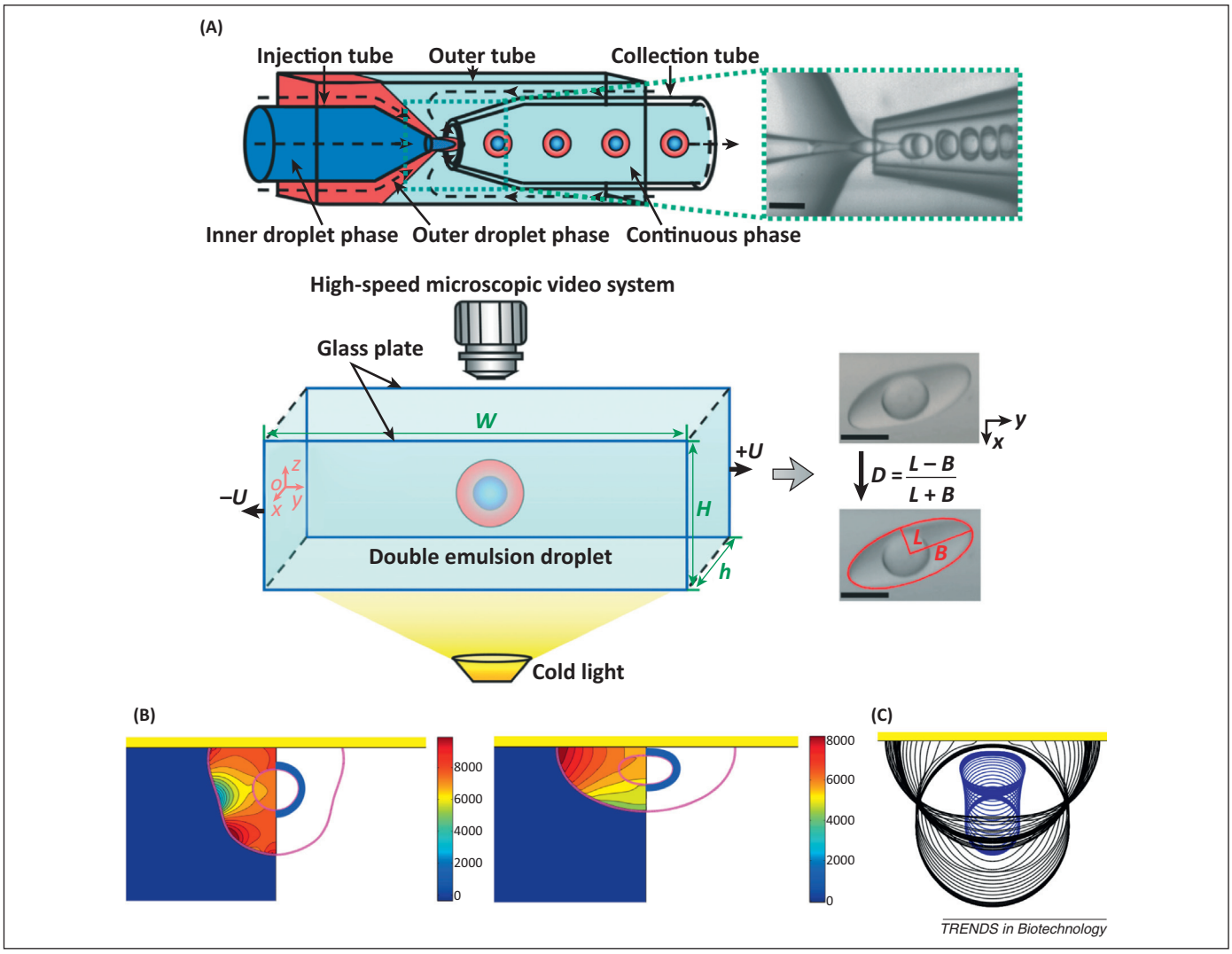

Figure 5. Computational model of digital (inkjet) printing. **(A)** Top: Sketch and image of the microcapillary double emulsion system of droplet generation. Scale bar, 300 μm. Bottom: Sketch of the experimental visualization of droplet deformation under shear (left panel) and the deformation parameter *D* (right panel). The red ellipsoidal profile in the right panel is programmatically the best-fit ellipse curve of the deformed droplet. Scale bar, 120 μm. **(B)** Simulation of forces associated with the cell-printing process. Pressure contours and pressure distribution on the cell were plotted on the left half and the right half, respectively. Governing nondimensional numbers are: We = 0.5, Re = 30, $d_o/d_i = 2.85$, $\sigma_o/\sigma_i = 2541$, $\mu_c/\mu_d = 10$. **(C)** Sequential boundaries of cell-encapsulating droplets on impact. (A) reproduced, with permission, from [61]. (B) and (C) reproduced, with permission, from [66].

shear stress with interface tension. The deformation, $D = (L - B)/(L + B)$, gives the degree of deformation of a droplet (D) as a function of the half-length (L) and half-breadth (B) of the best-fit ellipse approximating the droplet (Figure 5A). Experimental results along with computational simulations in this study provide a better understanding of hydrodynamic effects on the deformation of the double emulsion droplet [62], mimicking cell-encapsulating droplets.

Ejected cell-laden droplets experience significant hydrodynamic pressures, capillary forces, and shear stresses when landing on a substrate [63] (Figure 5B,C). When these mechanical stresses reach a certain threshold, cells may undergo apoptosis. However, these forces can be minimized by optimizing the ejection velocity or by changing the material properties of the encapsulating fluid. Cell fate may also depend on the hydrophobicity/hydrophilicity of the receiving surface, which is highly correlated with the contact angle between the droplet medium and the surface. Simulations can aid in predicting cell fate and provide more parametric control over 3D cancer models as well as complex viable tissue surrogates.

A finite-difference/front-tracking simulation model of viscous compound droplet deposition onto a receiving surface was presented as a model for cell printing [64–66]. Several parameters such as Weber number (We), diameter ratio (d_o/d_i), viscosity ratio (μ_c/μ_d), Reynolds number (Re), surface tension ratio (σ_o/σ_i), and equilibrium contact angle (ϑ_e) were studied to monitor cell deformation during cell printing. We and Re are widely used nondimensional numbers in fluid dynamics [67] that evaluate the influences of inertial forces compared with surface tension and viscous forces, respectively [68,69]. The computational results demonstrated that the geometric deformation of a cell monotonically increased: (i) as d_o/d_i decreased; (ii) as ϑ_e decreased; (iii) as σ_o/σ_i increased; (iv) as Re increased; or (v) as μ_c/μ_d decreased. A local minimum of predicted values for maximum geometric deformation was obtained at We = 2. Results demonstrated that ϑ_e and μ_c/μ_d were also strongly correlated with cell fate.

Next-generation models should incorporate non-Newtonian features of fluid flows [70,71], smaller contact angles, microstructured models of cells, and multiple patterning of droplets. Such computational models can accelerate the incorporation of bioprinting technologies into cancer research and help to develop more precise and reliable anticancer drug delivery systems.

Investigating cancer processes using bioprinting

Tumor heterogeneity

The heterogeneity and complexity of the tumor microenvironment can be replicated by co-printing bio-inks with different cell types, ECM, and biomolecules [33]. Heterologous constructs containing tumor cells, endothelial cells, and macrophages can be fabricated with a high degree of spatial control via bioprinting to replicate physiologically relevant cell–cell interactions. In these constructs, the initial cell density can also be controlled to closely mimic the high cell density of a tumor and replicate the cell–cell signaling that is known to have a significant role in cancer cell behavior [54]. In addition, co-printed 3D models of cancer cells and blood vessels allow real-time monitoring of the process of cancer metastasis, including tumor cell intravasation. A wide range of cancer types can be studied by printing different combinations of cancer cell types and surrounding cells to model cancer metastasis in a range of different tissue types, simply by reformulating the bio-ink. Biomolecule gradients, which play an important role in chemotaxis and cancer metastasis, can be generated using 3D printing methods to reveal molecular mechanisms of biochemical signaling [53,72,73].

Angiogenesis and tumor vasculature

One study proposed a novel method to examine cell behavior and screen potential new drugs. In this research, cancer and normal cells were seeded into 3D-printed biomimetic microstructures to study cell migration differences among cell types [74]. Here, 3D vascularization was achieved by printing a 3D microscaffold model based on a microcomputed tomography scan of rat capillaries in three different channel widths (25, 45, and 120 μm) to mimic the range of blood vessel diameters *in vivo*. These biomimetic models can be used to test the difference between normal and cancerous cell responses to antimigratory drugs [74].

Leaky (relatively permeable) [75,76] and poorly organized [77,78] vessel formation are distinctive features of cancerous tumors [79]. The notable differences between cancer and healthy vessels affect drug delivery in these tissues, necessitating that drug delivery be tested using leaky-vessel models to optimize the particle size and dosage of anticancer drugs [79,80]. Taking advantage of the spatial control over cell distribution using bioprinting, future work may aim to generate a 3D model for leaky vessels feeding a tumor compared with vessels in healthy tissue [54,79].

Tumor spheroid formation

3D projection printing has been used to generate concave PEG structures that form and maintain breast cancer spheroids [81]. The 3D projection printing technique was modified by the use of nonlinear UV light and a circular gradient exposure pattern such that the center receives little UV exposure relative to the edge of the circle, generating 3D concave structures. When BT474 breast cancer cells were seeded on these structures, spheroids formed with a narrow distribution of size compared with flat cultures. These spheroids exhibited hollow necrotic cores with high expression of HIF-1α, a biomarker for hypoxia, which is consistent with results previously observed for tumor spheroids. This 3D-printed platform may serve as a low-cost, highly reproducible, physiologically relevant tumor model for studying tumor progression, migration, and angiogenesis with the ability to maintain spheroids in long-term culture.

Bioprinting for anticancer drug development

Initial work using bioprinting to create 3D models for drug development includes the printing of cell-laden Matrigel constructs and incorporation of these constructs into microfluidic devices [82]. This study focused on multicellular prodrug conversion and liver radioprotection using the prodrug amifostine, which is a drug precursor carrying a parent compound to enhance solubility and targeting before conversion into the active form. The fabrication method was based on temperature-controlled bioprinting of pre-gels (such as Matrigel and collagen) into prefabricated PDMS substrates [82]. Progress in this field led to bioprinting technologies being used for anticancer drug development by creating physiologically relevant 3D human carcinoma models [12,83].

To establish novel treatments and acquire FDA approval for new drugs, studies conducted in conventional ways may extend up to 15 years and require a budget of US$2.6 billion [Bright Focus Foundation (2014) Understanding clinical trials (http://www.brightfocus.org/understanding-clinical-trials-overview.html); Peters, S. and Lowy, P. (2014) Cost to develop and win marketing approval for a new drug is $2.6 billion. Tufts Center for the Study of Drug Development (http://csdd.tufts.edu/news/complete_story/pr_tufts_csdd_2014_cost_study)]. Ultimately, one in five proposed drugs that reach clinical testing obtain FDA approval [Bright Focus Foundation (2014) Understanding clinical trials (http://www.brightfocus.org/understanding-clinical-trials-overview.html)]. In addition, the results from testing on animal models may not accurately predict the result in human testing due to cross-species differences [84], causing many drugs to fail in the clinical trial stage. Furthermore, animal testing raises ethical concerns and this ethical framework is closely regulated to control the use of animals for scientific research [85].

3D-bioprinted tumor models are excellent candidates to replace or supplement animal testing before human trials, as bioprinting enables repeatability of testing, close biomimicry, and high-throughput fabrication capabilities. New drug delivery systems can be tested for the biodegradability of drug carriers such as polymer microspheres and drug-release kinetics using *in vitro* cancer models before animal or human testing [80,86]. The efficacy of a drug treatment *in vivo* can be well predicted by examining its effect on the bioprinted model. The repeatability of bioprinting 3D cancer models contributes to the development of 3D-printed cancer models as an industry standard [87].

Concluding remarks and future perspectives

Here we discuss recently developed 3D printing techniques to emulate a 3D tumor environment. A key advantage of the 3D microenvironment over traditional 2D cell culture is the ability to obtain more accurate and reliable data from the model. Studies using 3D *in vitro* cancer models rather than 2D models show greater cell viability, more physiologically relevant protein expression profiles, higher proliferation rate, higher chemoresistance to anticancer drugs, and characteristics of real tumors (e.g., presence of necrotic cores). Bioprinting of heterologous cells in 3D has the potential for better *in vitro* modeling of the tumor microenvironment with high viability and 3D control over the spatial distribution of cells. High-throughput fabrication helps to better characterize tumor formation, progression, and response to anticancer therapies [12].

The absence of a direct correlation between the genetics and physiology of animal models and humans currently limits our understanding of how cancer cells behave in humans. Living microarchitectures bioprinted from human cells are more realistic for creating disease models. In the interest of developing more effective anticancer treatments, an ample amount of information remains to be discovered and these studies can be accelerated using bioprinted cancer models. Current bioprinting applications for cancer research are promising to establish new experimental procedures for the fabrication of 3D cancer models to pursue new discoveries in cancer biology or test clinical therapeutics. Further studies in bioprinting will enable high-throughput fabrication of 3D cancer models for elucidating the underlying mechanisms of cancer progression, studying cancer cell behavior, screening drugs, and developing effective clinical treatments.

These modeling systems have the potential to be the experimental bridges to new clinical techniques by which a tumor model specific to a patient can be created *in vitro*. Bio-inks can be generated by proliferating cancer cells taken from a donated tumor sample or a tumor bank. After printing with these bio-inks, cells form their natural network and tumor tissue, on which new cancer drugs and treatments can be tested [John, G. (2013) Organovo using 3D bioprinting to push cancer research to new levels (http://www.3dprinterworld.com/article/organovo-using-3d-bioprinting-push-cancer-research-new-levels)]. This would make it possible to test drug therapies *in vitro*, giving information about the most effective drug type and dosage and developing a personalized cancer treatment for the patient.

Acknowledgments

S.T. acknowledges the UConn Research Excellence Program Award.

References

1 Stewart, B.W. and Wild, C.P., eds (2014) *(2014) World Cancer Report*, IARC
2 Berger, M.F. *et al.* (2011) The genomic complexity of primary human prostate cancer. *Nature* 470, 214–220
3 Palanisamy, N. *et al.* (2010) Rearrangements of the RAF kinase pathway in prostate cancer, gastric cancer and melanoma. *Nat. Med.* 16, 793–798
4 Ridky, T.W. *et al.* (2010) Invasive three-dimensional organotypic neoplasia from multiple normal human epithelia. *Nat. Med.* 16, 1450–1455
5 Ghosh, S. *et al.* (2005) Three-dimensional culture of melanoma cells profoundly affects gene expression profile: a high density oligonucleotide array study. *J. Cell. Physiol.* 204, 522–531
6 Kim, B.J. *et al.* (2013) Cooperative roles of SDF-1α and EGF gradients on tumor cell migration revealed by a robust 3D microfluidic model. *PLoS ONE* 8, e68422
7 Zervantonakis, I.K. *et al.* (2012) Three-dimensional microfluidic model for tumor cell intravasation and endothelial barrier function. *Proc. Natl. Acad. Sci. U.S.A.* 109, 13515–13520
8 Friedl, P. and Wolf, K. (2010) Plasticity of cell migration: a multiscale tuning model. *J. Cell Biol.* 188, 11–19
9 Li, C.L. *et al.* (2008) Survival advantages of multicellular spheroids vs. monolayers of HepG2 cells *in vitro*. *Oncol. Rep.* 20, 1465–1471
10 Chopra, V. *et al.* (1997) Three-dimensional endothelial-tumor epithelial cell interactions in human cervical cancers. *In Vitro Cell. Dev. Biol. Anim.* 33, 432–442
11 Loessner, D. *et al.* (2010) Bioengineered 3D platform to explore cell–ECM interactions and drug resistance of epithelial ovarian cancer cells. *Biomaterials* 31, 8494–8506
12 Zhao, Y. *et al.* (2014) Three-dimensional printing of HeLa cells for cervical tumor model in vitro. *Biofabrication* 6, 035001
13 Wang, C. *et al.* (2014) Three-dimensional *in vitro* cancer models: a short review. *Biofabrication* 6, 022001
14 Kruth, J-P. (1991) Material incress manufacturing by rapid prototyping techniques. *CIRP Ann. Manuf. Techn.* 40, 603–614
15 Heller, T.B. *et al.* Quadrax Corp. Method of and apparatus for forming a solid three-dimensional article from a liquid medium, WO 1991012120 A1
16 Freedman, D.H. (2012) Layer by layer. *Technol. Rev.* 115, 50–53
17 Demirci, U. and Montesano, G. (2007) Single cell epitaxy by acoustic picolitre droplets. *Lab Chip* 7, 1139–1145
18 Mironov, V. *et al.* (2003) Organ printing: computer-aided jet-based 3D tissue engineering. *Trends Biotechnol.* 21, 157–161
19 Moon, S. *et al.* (2010) Layer by layer three-dimensional tissue epitaxy by cell-laden hydrogel droplets. *Tissue Eng. Part C Methods* 16, 157–166
20 Xu, F. *et al.* (2010) A droplet-based building block approach for bladder smooth muscle cell (SMC) proliferation. *Biofabrication* 2, 014105
21 Mironov, V. *et al.* (2008) Organ printing: promises and challenges. *Regen. Med.* 3, 93–103
22 Hamid, Q. *et al.* (2011) Fabrication of three-dimensional scaffolds using precision extrusion deposition with an assisted cooling device. *Biofabrication* 3, 034109
23 Tasoglu, S. and Demirci, U. (2013) Bioprinting for stem cell research. *Trends Biotechnol.* 31, 10–19
24 Tasoglu, S. *et al.* (2014) Untethered micro-robotic coding of three-dimensional material composition. *Nat. Commun.* 5, 3124
25 Tasoglu, S. *et al.* (2014) Guided and magnetic self-assembly of tunable magnetoceptive gels. *Nat. Commun.* 5, 4702
26 Tasoglu, S. *et al.* (2015) Magnetic levitational assembly for living material fabrication. *Adv. Healthc. Mater.* Published online April 14, 2015. http://dx.doi.org/10.1002/adhm.201500092
27 Guven, S. *et al.* (2015) Multiscale assembly for tissue engineering and regenerative medicine. *Trends Biotechnol.* 33, 269–279
28 Chen, P. *et al.* (2014) Microscale assembly directed by liquid-based template. *Adv. Mater.* 26, 5936–5941
29 Tasoglu, S. *et al.* (2013) Paramagnetic levitational assembly of hydrogels. *Adv. Mater.* 25, 1137–1143 1081
30 Xu, F. *et al.* (2011) Three-dimensional magnetic assembly of microscale hydrogels. *Adv. Mater.* 23, 4254–4260
31 Xu, F. *et al.* (2011) The assembly of cell-encapsulating microscale hydrogels using acoustic waves. *Biomaterials* 32, 7847–7855
32 Gurkan, U.A. *et al.* (2012) Emerging technologies for assembly of microscale hydrogels. *Adv. Healthc. Mater.* 1, 149–158
33 Junttila, M.R. and de Sauvage, F.J. (2013) Influence of tumour microenvironment heterogeneity on therapeutic response. *Nature* 501, 346–354
34 Boland, T. *et al.* (2006) Application of inkjet printing to tissue engineering. *Biotechnol. J.* 1, 910–917
35 Nakamura, M. *et al.* (2005) Biocompatible inkjet printing technique for designed seeding of individual living cells. *Tissue Eng.* 11, 1658–1666
36 Fedorovich, N.E. *et al.* (2009) Evaluation of photocrosslinked Lutrol hydrogel for tissue printing applications. *Biomacromolecules* 10, 1689–1696

37 Chang, C.C. *et al.* (2011) Direct-write bioprinting three-dimensional biohybrid systems for future regenerative therapies. *J. Biomed. Mater. Res. B: Appl. Biomater.* 98, 160–170
38 Khalil, S. and Sun, W. (2007) Biopolymer deposition for freeform fabrication of hydrogel tissue constructs. *Mater. Sci. Eng. C* 27, 469–478
39 Chang, R. *et al.* (2008) Effects of dispensing pressure and nozzle diameter on cell survival from solid freeform fabrication-based direct cell writing. *Tissue Eng. Part A* 14, 41–48
40 Odde, D.J. and Renn, M.J. (1999) Laser-guided direct writing for applications in biotechnology. *Trends Biotechnol.* 17, 385–389
41 Nahmias, Y. *et al.* (2005) Laser-guided direct writing for three-dimensional tissue engineering. *Biotechnol. Bioeng.* 92, 129–136
42 Guillotin, B. *et al.* (2010) Laser assisted bioprinting of engineered tissue with high cell density and microscale organization. *Biomaterials* 31, 7250–7256
43 Gaebel, R. *et al.* (2011) Patterning human stem cells and endothelial cells with laser printing for cardiac regeneration. *Biomaterials* 32, 9218–9230
44 Barron, J.A. *et al.* (2004) Application of laser printing to mammalian cells. *Thin Solid Films* 453, 383–387
45 Cohen, D.L. *et al.* (2006) Direct freeform fabrication of seeded hydrogels in arbitrary geometries. *Tissue Eng.* 12, 1325–1335
46 Jakab, K. *et al.* (2006) Three-dimensional tissue constructs built by bioprinting. *Biorheology* 43, 509–513
47 Visser, J. *et al.* (2013) Biofabrication of multi-material anatomically shaped tissue constructs. *Biofabrication* 5, 035007
48 Nahmias, Y. and Odde, D.J. (2006) Micropatterning of living cells by laser-guided direct writing: application to fabrication of hepatic-endothelial sinusoid-like structures. *Nat. Protoc.* 1, 2288–2296
49 Colina, M. *et al.* (2006) Laser-induced forward transfer of liquids: study of the droplet ejection process. *J. Appl. Phys.* 99, 7
50 Kattamis, N.T. *et al.* (2009) Laser direct write printing of sensitive and robust light emitting organic molecules. *Appl. Phys. Lett.* 94, 3
51 Lu, Y. *et al.* (2006) A digital micro-mirror device-based system for the microfabrication of complex, spatially patterned tissue engineering scaffolds. *J. Biomed. Mater. Res. A* 77, 396–405
52 Soman, P. *et al.* (2012) Cancer cell migration within 3D layer-by-layer microfabricated photocrosslinked PEG scaffolds with tunable stiffness. *Biomaterials* 33, 7064–7070
53 Dababneh, A.B. and Ozbolat, I.T. (2014) Bioprinting technology: a current state-of-the-art review. *J. Manuf. Sci. Eng.* 136, 061016
54 Xu, F. *et al.* (2011) A three-dimensional *in vitro* ovarian cancer coculture model using a high-throughput cell patterning platform. *Biotechnol. J.* 6, 204–212
55 Murphy, S.V. and Atala, A. (2014) 3D bioprinting of tissues and organs. *Nat. Biotechnol.* 32, 773–785
56 Chung, S. *et al.* (2010) Microfluidic platforms for studies of angiogenesis, cell migration, and cell–cell interactions. *Ann. Biomed. Eng.* 38, 1164–1177
57 Nguyen-Ngoc, K.V. *et al.* (2012) ECM microenvironment regulates collective migration and local dissemination in normal and malignant mammary epithelium. *Proc. Natl. Acad. Sci. U.S.A.* 109, E2595–E2604
58 King, S.M. *et al.* (2014) Development of 3D bioprinted human breast cancer for *in vitro* drug screening. *Cancer Res.* 74, 2034
59 Kolesky, D.B. *et al.* (2014) 3D bioprinting of vascularized, heterogeneous cell-laden tissue constructs. *Adv. Mater.* 26, 3124–3130
60 Hansen, C.J. *et al.* (2013) High-throughput printing via microvascular multinozzle arrays. *Adv. Mater.* 25, 96–102
61 Chen, Y. *et al.* (2015) Enhancing and suppressing effects of an inner droplet on deformation of a double emulsion droplet under shear. *Lab Chip* 15, 1255–1261
62 Utada, A.S. *et al.* (2005) Monodisperse double emulsions generated from a microcapillary device. *Science* 308, 537–541
63 Demirci, U. and Montesano, G. (2007) Cell encapsulating droplet vitrification. *Lab Chip* 7, 1428–1433
64 Berg, J.C. (ed.) (1993) *Wettability*, Marcel Dekker
65 Muradoglu, M. and Tasoglu, S. (2010) A front-tracking method for computational modeling of impact and spreading of viscous droplets on solid walls. *Comput. Fluids* 39, 615–625
66 Tasoglu, S. *et al.* (2010) Impact of a compound droplet on a flat surface: a model for single cell epitaxy. *Phys. Fluids* 22, 082103
67 Tasoglu, S. *et al.* (2013) Transient swelling, spreading and drug delivery by a dissolved anti-HIV microbicide-bearing film. *Phys. Fluids* 25, 031901
68 Tasoglu, S. *et al.* (2011) The effects of inhomogeneous boundary dilution on the coating flow of an anti-HIV microbicide vehicle. *Phys. Fluids* 23, 093101
69 Tasoglu, S. *et al.* (2008) The effect of soluble surfactant on the transient motion of a buoyancy-driven bubble. *Phys. Fluids* 20, 040805
70 Tasoglu, S. *et al.* (2011) The consequences of yield stress on deployment of a non-Newtonian anti-HIV microbicide gel. *J. Nonnewton. Fluid Mech.* 166, 1116–1122
71 Tasoglu, S. *et al.* (2012) Transient spreading and swelling behavior of a gel deploying an anti-HIV microbicide. *J. Nonnewton. Fluid Mech.* 187, 36–42
72 Keenan, T.M. and Folch, A. (2008) Biomolecular gradients in cell culture systems. *Lab Chip* 8, 34–57
73 Weiss, L.E. *et al.* (2005) Bayesian computer-aided experimental design of heterogeneous scaffolds for tissue engineering. *Comput. Aided Des.* 37, 1127–1139
74 Huang, T.Q. *et al.* (2014) 3D printing of biomimetic microstructures for cancer cell migration. *Biomed. Microdevices* 16, 127–132
75 Hobbs, S.K. *et al.* (1998) Regulation of transport pathways in tumor vessels: role of tumor type and microenvironment. *Proc. Natl. Acad. Sci. U.S.A.* 95, 4607–4612
76 Yuan, F. *et al.* (1994) Microvascular permeability and interstitial penetration of sterically stabilized (stealth) liposomes in a human tumor xenograft. *Cancer Res.* 54, 3352–3356
77 Baish, J.W. *et al.* (2011) Scaling rules for diffusive drug delivery in tumor and normal tissues. *Proc. Natl. Acad. Sci. U.S.A.* 108, 1799–1803
78 Nagy, J.A. *et al.* (2009) Why are tumour blood vessels abnormal and why is it important to know? *Br. J. Cancer* 100, 865–869
79 Chauhan, V.P. *et al.* (2012) Normalization of tumour blood vessels improves the delivery of nanomedicines in a size-dependent manner. *Nat. Nanotechnol.* 7, 383–388
80 He, Z.Q. and Xiong, L.Z. (2011) Fabrication of poly(D,L-lactide-co-glycolide) microspheres and degradation characteristics in vitro. *J. Macromol. Sci. Part B: Phy.* 50, 1682–1690
81 Hribar, K.C. *et al.* (2015) Nonlinear 3D projection printing of concave hydrogel microstructures for long-term multicellular spheroid and embryoid body culture. *Lab Chip* 15, 2412–2418
82 Snyder, J.E. *et al.* (2011) Bioprinting cell-laden matrigel for radioprotection study of liver by pro-drug conversion in a dual-tissue microfluidic chip. *Biofabrication* 3, 034112
83 Unger, C. *et al.* (2014) Modeling human carcinomas: physiologically relevant 3D models to improve anti-cancer drug development. *Adv. Drug Deliv. Rev.* 79–80, 50–67
84 Runge, A. *et al.* (2014) An inducible hepatocellular carcinoma model for preclinical evaluation of antiangiogenic therapy in adult mice. *Cancer Res.* 74, 4157–4169
85 Festing, S. and Wilkinson, R. (2007) The ethics of animal research. Talking point on the use of animals in scientific research. *EMBO Rep.* 8, 526–530
86 Singh, M. *et al.* (2008) Microsphere-based seamless scaffolds containing macroscopic gradients of encapsulated factors for tissue engineering. *Tissue Eng. Part C Methods* 14, 299–309
87 Demirbag, B. *et al.* (2011) Advanced cell therapies with and without scaffolds. *Biotechnol. J.* 6, 1437–1453
88 Guillemot, F. *et al.* (2010) High-throughput laser printing of cells and biomaterials for tissue engineering. *Acta Biomater* 6, 2494–2500
89 Malda, J. *et al.* (2013) 25th anniversary article: Engineering hydrogels for biofabrication. *Adv Mater* 25, 5011–5028